Eur Biophys J (2000) 29: 29–37

ARTICLE

Charlotte Adcock · Graham R. Smith
Mark S.P. Sansom

The nicotinic acetylcholine receptor: from molecular model to single-channel conductance

Received: 2 August 1999 / Revised version: 5 November 1999 / Accepted: 9 November 1999

Abstract The nicotinic acetylcholine receptor (nAChR) is the archetypal ligand-gated ion channel. A model of the α7 homopentameric nAChR is described in which the pore-lining M2 helix bundle is treated atomistically and the remainder of the molecule is treated as a "low resolution" cylinder. The surface charge on the cylinder is derived from the distribution of charged amino acids in the amino acid sequence (excluding the M2 segments). This model is explored in terms of its predicted single-channel properties. Based on electrostatic potential profiles derived from the model, the one-dimensional Poisson-Nernst-Planck equation is used to calculate single-channel current/voltage curves. The predicted single-channel conductance is three times higher (ca. 150 pS) than that measured experimentally, and the predicted ion selectivity agrees with the observed cation selectivity of nAChR. Molecular dynamics (MD) simulations are used to estimate the self-diffusion coefficients (D) of water molecules within the channel. In the narrowest region of the pore, D is reduced ca. threefold relative to that of bulk water. Assuming that the diffusion of ions scales with that of water, this yields a revised prediction of the single-channel conductance (ca. 50 pS) in good agreement with the experimental value. We conclude that combining atomistic (MD) and continuum electrostatics calculations is a promising approach to bridging the gap between structure and physiology of ion channels.

Key words Ion channel · Electrostatics · Simulation · Molecular dynamics · Water · Diffusion

C. Adcock · G.R. Smith · M.S.P. Sansom (✉)
Laboratory of Molecular Biophysics,
The Rex Richards Building,
Department of Biochemistry,
University of Oxford, South Parks Road,
Oxford OX1 3QU, UK
e-mail: mark@biop.ox.ac.uk

Introduction

The nicotinic acetylcholine receptor channel (nAChR) is the best understood member of a family of neurotransmitter gated ion channels which also includes receptors for glycine, GABA and serotonin (Barnard 1992; Ortells and Lunt 1995). It is selective for cations over anions, and has a relatively high single-channel conductance (ca. 50 pS). Unlike the situation with K channels (Doyle et al. 1998), we do not yet possess a near atomic resolution crystallographic structure for this channel. However, combining cryoelectron microscopy results (Unwin 1993, 1995; Miyazawa et al. 1999) with mutagenesis and protein chemistry data (Changeux et al. 1992; Lester 1992; Bertrand et al. 1993; Galzi and Changeux 1994; Hucho et al. 1996) enables one to construct both secondary structure (Le Novère et al. 1999) and three-dimensional models (Ortells et al. 1996; Sankararamakrishnan et al. 1996; Tikhonov and Zhorov 1998) of the pore formed by the nAChR. In particular, it has been established that the lining of the transbilayer pore is formed principally by a pentameric bundle of M2 helices packed in a pseudo-symmetric (e.g. in the muscle type nAChR, $\alpha_2\beta\gamma\delta$) or symmetric (in some neuronal nAChR, e.g. $\alpha7_5$) fashion around a central water-filled pore. The M2 helix is apparently the second transmembrane segment of each of the five subunits which make up the intact nAChR. A wide range of studies (Changeux et al. 1992; Lester 1992; Hucho et al. 1996) have identified the M2 residues whose sidechains appear to line the pore. In this paper we will concern ourselves with M2 from the neuronal α7 type nAChR. This can, at least in vitro, form homopentameric nAChR in which the pore is lined by five identical M2 helices, thus simplifying modelling and simulation studies. The sequence of M2α7 used in this paper is:

Ala-*Asp*$^{-4}$-Ser-Gly-*Glu*$^{-1}$-Lys-Ile-*Ser*$^{+2}$-Leu-Gly-Ile-*Thr*$^{+6}$-Val-Leu-Leu-*Ser*$^{+10}$-Leu-Thr-Val-Phe-Met-Leu-Leu-Val-Ala-*Glu*$^{+20}$

Note that we number the M2 sequence according to the scheme used previously (Lester 1992; Adcock et al. 1998), and that the pore-lining polar sidechains are indicated by italics.

One aim of computational studies of ion channels is to be able to relate structure to function. In particular, one would like to be able to start with an atomic resolution model of an ion channel and to compute physiological properties such as single-channel conductance and ion selectivity. However, this is non-trivial. Although atomistic molecular dynamics (MD) simulations, for example, provide information on the dynamics and energetics of ions and water within a channel (Chiu et al. 1991, 1993; Roux and Karplus 1994; Roux 1995; Breed et al. 1996; Smith and Sansom 1997, 1998, 1999), the discrepancy between the timescale of MD simulations (ca. 1 ns) and the timescale of ion permeation (ca. 0.1 μs) means that a hierarchy of computational approaches, corresponding to different timescales, will be required to build a bridge from structural biology to physiology (Cooper et al. 1985; Chung et al. 1998; Roux 1998). One approach is to use MD simulations to obtain a short timescale picture of channel/ion/water interactions and to use continuum electrostatics calculations and diffusion-based simulations to address ion permeation. Continuum electrostatics calculations, in different forms, have been used with some success to predict single-channel current-voltage relationships for channels formed by simple peptides (Kienker et al. 1994; Chen et al. 1997; Lear et al. 1997; Woolley et al. 1997; Dieckmann et al. 1999; Chung et al. 1999) and by porins (Dutzler et al. 1999).

In a previous paper (Adcock et al. 1998) we described a model of the nAChR pore in which the $M2_5$ bundle was embedded in a low-resolution model of the remainder of the protein, and showed how this model could be used to calculate electrostatic potential energy profiles along the pore. In this paper we extend this work to calculate single-channel current-voltage relationships. By combining this approach with an atomistic simulation of water dynamics within the channel, we show how such a simple model may account for the magnitude of the channel conductance, and for the ion selectivity of the nAChR.

Methods

Model building

The helix bundle and helix bundle plus cylinder models were generated as described in previous papers (Adcock et al. 1998; Sansom et al. 1998). Briefly, simulated annealing via restrained MD (Kerr et al. 1994; Sansom et al. 1995) was used to build the $M2_5$ helix bundle. Target restraints were used to restrain the M2 α-helices to their approximate positions as defined by the 9 Å resolution electron microscopic image of the pore (Unwin 1995). Intra-helix restraints were imposed to maintain the hydrogen bonding pattern of each M2 α-helix. Inter-helix restraints were used to orient pore-lining sidechains towards the centre of the helix bundle.

An irregular cylinder model of the remainder of the channel protein was generated from a simple cubic lattice of atoms with a spacing of 2.5 Å. The dimensions of the irregular cylinder were determined from electron microscope images of the nAChR (Toyoshima and Unwin 1988; Unwin 1993, 1995). Net charges on the relevant domains (extracellular, transmembrane, intracellular) were calculated from the amino acid sequence of α7, excluding the M2 sequence and assuming full ionisation of acidic and basic sidechains (a charge of $+0.5$ was used for His). Charges on each region were distributed evenly over the dummy atoms forming the inner/outer surfaces of each cylinder. The $M2_5$ helix bundle was embedded into the transmembrane (TM) region of the cylinder model, discarding any cylinder atoms too close to M2 atoms.

Having generated this model, the pK_A values of ionisable sidechains within the M2 helices were calculated as described previously (Adcock et al. 1998). Thus, all of the Asp^{-4}, Glu^{-1} and Lys^{0} sidechains were ionised, whereas all of the Glu^{+20} residues were protonated (i.e. in their neutral state).

Continuum electrostatics

The electrostatic potential ($F\Phi$) was calculated by solving the linearised Poisson-Boltzmann equation. A low dielectric slab of thickness ca. 40 Å, into which the channel models were inserted, was used to mimic the lipid bilayer. The channel and "membrane" slab volumes were defined by their solvent accessible surface and were assigned a dielectric of 4. As discussed elsewhere (e.g. Ullmann and Knapp 1999), there is some debate concerning the appropriate value of the protein dielectric. Simonson and Perahia (1995) have shown that for globular proteins the dielectric varies from ca. 20 at the surface to ca. 4 in the hydrophobic core. Thus, for a membrane protein a value of 4 seems more appropriate. Furthermore, a value of 4 has given reasonable correlation with experiment in calculations on ion channels formed by the peptide alamethicin (Woolley et al. 1997). Both the solvent within the pore and the bulk solvent were assigned a dielectric of 78. An ionic strength of 100 mM (monovalent ions) and a Stern radius of 2 Å were used.

Current-voltage curves

The one-dimensional Poisson-Nernst-Planck equation (Hille 1992) was used to calculate single-channel current-voltage curves. The equation is effectively the diffusion equation for charged particles. It describes the mean flux along the channel pore axis as a function of concentration and electric potential; J_i is the mean particle flux, C_i

is concentration, F is Faraday's constant, ϕ is the electric potential, z is the distance along the pore axis and q_i is the ionic valence:

$$J_i = -D_i\left[\frac{\mathrm{d}C_i(z)}{\mathrm{d}z} + \frac{q_iF}{RT}C_i\frac{\mathrm{d}\phi}{\mathrm{d}z}\right] \quad (1)$$

Integration of Eq. (1) leads to Eq. (2) from which the total current per channel, I, may be calculated:

$$I = -AF\sum_i C_iq_iD_i\frac{\exp\left(\frac{q_iF\Delta\phi_{\mathrm{TM}}}{RT}\right)-1}{\int_{z=s}^{z=s+1}\exp\left(\frac{q_iF(\phi_{\mathrm{CHANNEL}}(z)+\phi_{\mathrm{TM}}(z))}{RT}\right)\mathrm{d}z} \quad (2)$$

C_i is the concentration of ionic species i which has valence q_i and diffusion coefficient D_i; A is the cross-sectional area of the channel; $\Delta\phi_{\mathrm{TM}}$ is the TM potential (i.e. the voltage, V) and $\phi_{\mathrm{CHANNEL}}(z)$ and $\phi_{\mathrm{TM}}(z)$ are the electrostatic potential due to the channel and the TM potential at point z (along the channel axis), respectively. Note that the potential in Eq. (1) is given by $\phi(z) = \phi_{\mathrm{CHANNEL}}(z) + \phi_{\mathrm{TM}}(z)$.

MD simulations

MD simulations of solvated channel models were performed using similar methods to those described previously (Smith and Sansom 1997). Both of the channel models were solvated using a pre-equilibrated box of modified TIP3P waters. The $M2_5$ model was solvated using an hourglass-shaped volume of waters defined to extend ca. 12 Å above the top and bottom of the channel, producing caps of water at either end. The final solvated structure contained 1557 water molecules. The $M2_5$ + cyl model was solvated using a cylindrical volume of water molecules of length ca. 120 Å, resulting in a solvated structure containing 1369 water molecules. The water molecules extended as far as the top and bottom layers of dummy atoms forming the cylinder.

In the simulations, only polar hydrogens were represented explicitly. Non-bonded interactions, i.e. van der Waals and electrostatic interactions, were cut off at 14 Å using a shift function. The dummy atoms forming the cylinder model were fixed throughout the simulation. $M2_5$ Cα atoms in both models were harmonically restrained throughout the simulation, using a force constant of 10 kcal mol^{-1} Å^{-2}. Previous simulations (Breed et al. 1996; Smith and Sansom 1997) have shown it is advisable to restrain the water molecules at each end of the system during the simulation. Planar restraints were imposed at either end of the $M2_5$ + cyl model in order to prevent water from escaping from either end of the cylinder. After energy minimisation and equilibration of the system, a 500 ps production simulation was run. Water self-diffusion coefficients and dipole moment projects were calculated as described previously (Breed et al. 1996; Smith and Sansom 1997).

The model/water coordinates from the end of the 500 ps production run were used as a starting point for the model/water/ion simulations. Simulations were performed in which a Na^+ ion was placed at points along the pore (z) axis. Fourteen simulations were run for the $M2_5$ + cyl model, with the ion positioned between $z = -35$ Å and $z = +30$ Å at 5 Å spacings. In each simulation, the ion was inserted at its position on the pore axis and the nearest water molecule to it was removed. The ion was harmonically restrained to its initial z-coordinate throughout the simulation with a force constant of 10 kcal mol^{-1} Å^{-2}. Each simulation consisted of a minimisation, heating (6 ps) and equilibration stage (9 ps). Interaction energies between the ion and model or ion and water were obtained from the 9 ps equilibration. This is a rather short simulation period, but simulations on a number of systems suggest that the errors in the potential energy introduced by this are commensurate with the approximate model used in the calculations. For the purpose of this analysis the non-bonded cut-off was extended to 30 Å. The interaction energy of a Na^+ ion with bulk water (Smith and Sansom 1997) was subtracted from all ion-x interaction energies in which water molecules formed a component of x.

Computational details

Model building used Xplor V3.1 (Brünger 1992). Quanta 4.1 (MSI) was used in the generation of the cylinder model and preparation of structure diagrams. All electrostatics calculations employed UHBD version 5.1 (Davis et al. 1991) (with some local modifications) and partial atomic charges from the Quanta/Charmm22 parameter set. Simulations were performed using CHARMm23 (Brooks et al. 1983) with the param19 parameter set. All calculations were carried out on Silicon Graphics workstations or on a R10 K Silicon Graphics Origin2000.

Results and discussion

Model of the channel

The model consists of a bundle of five M2α7 helices ($M2_5$) embedded in an irregular cylinder which corresponds to the overall envelope of the protein as seen in low-resolution electron microscopy images (Toyoshima and Unwin 1988; Unwin 1993). The $M2_5$ bundle (Fig. 1A) was constructed, as described previously (Adcock et al. 1998), so as to fit the density in the electron microscopy images (Unwin 1995), with the pore-lining residues (Glu^{-1}, Ser^{+2}, Thr^{+6} and Ser^{+10}) directed towards the centre of the bundle. This model was then embedded in the irregular cylinder (Fig. 1B). The cylinder is 110 Å long, with an inner radius of 10 Å and an outer radius of 30 Å. The intracellular (IC)

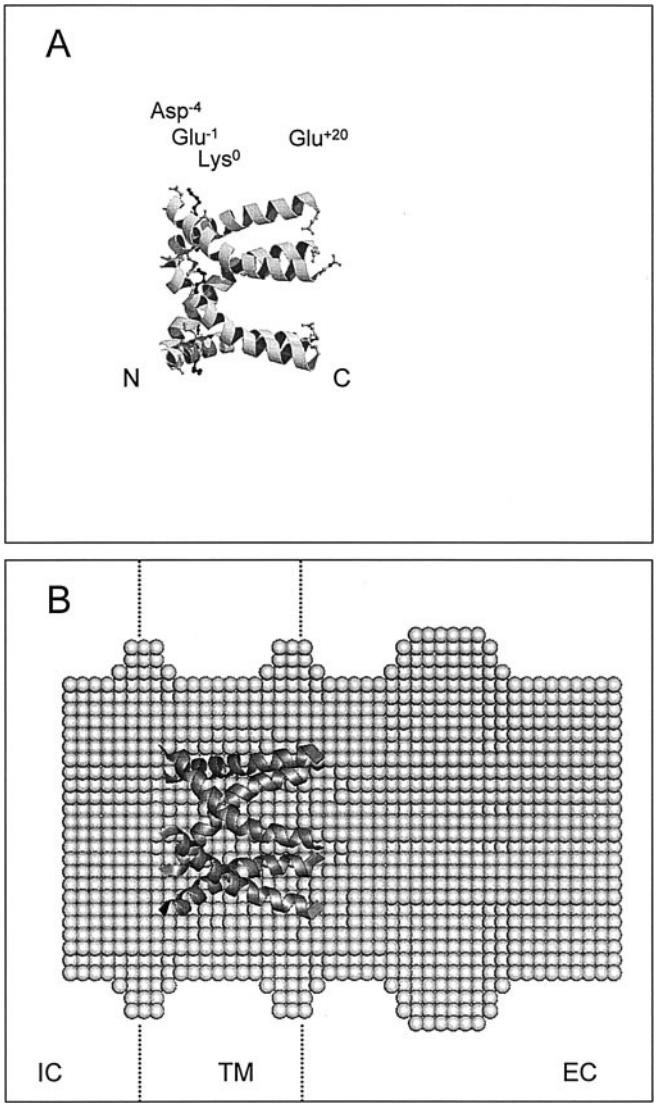

Fig. 1 **A** Model of the $M2_5$ helix bundle, viewed perpendicular to the pore axis. The intracellular (N-terminal) mouth of the pore is on the left-hand side of the diagram, which shows the M2 helices in "ribbons" format. The acidic and basic sidechains are shown in *light* and *dark grey*, respectively [diagram prepared using Molscript (Kraulis 1991) and Raster3D (Merritt and Bacon 1997)]. **B** The $M2_5$ + cyl model, in which the $M2_5$ helix bundle shown in **A** (*dark grey*) is embedded in an irregular cylindrical pore of van der Waals spheres (*light grey*) which mimics the dimensions of the overall envelope of the nAChR protein. The approximate location of the bilayer is shown by the *broken lines*. *IC* = intracellular; *TM* = transmembrane; *EC* = extracellular

section runs from z ca. −40 to −15 Å, the TM section from z ca. −15 to +15 Å, and the extracellular (EC) section from z ca. +15 to +80 Å. The surface of the cylinder was assigned a charge based on the proposed topology of the nAChR and its amino acid sequence, assuming charges of +1 for all Lys and Arg, −1 for all Glu and Asp, and 0.5 for all His residues. For the three regions defined above, the resultant total surface charges are: IC, $\sum q = +2.5$e; TM, $\sum q = -5.0$e; and EC, $\sum q = -17.5$e (where the charges are per channel, i.e. per pentamer) (the M2 α-helices were excluded from the calculation of $\sum$q for the TM region). The surface charge density was the same for the inner and outer surfaces of the cylinder in a given region. The most negative surface charge density was ca. -10^{-3} e Å^{-2} (for the EC domain).

It should be noted that in this model the only regions represented atomistically are the M2 helices. All other residues are represented by the cylinder. Thus, the M1-M2 loops, which have been suggested (Corringer et al. 1999; Le Novère et al. 1999) to play a key role in selectivity, are not modelled atomistically. This is not really possible without further information on the conformation of this region.

Potential profiles

The electrostatic potential profiles (calculated as the energy of a +1e probe charge moved along the central pore axis) for the pore model and its components are shown in Fig. 2A. The profiles for the helix bundle on its own ($M2_5$) and for the helix bundle in the charged cylinder ($M2_5$ + cyl) are as presented in Adcock et al. (1998). Additional analysis presented here is the profile for $M2_5$ + cyl_0. This corresponds to a calculation in which the $M2_5$ bundle was embedded in the cylinder, but the latter was assigned a zero surface charge. It can be seen that the effect of the low dielectric ($\varepsilon = 4$) cylinder surrounding the helix bundle is to "focus" the electrostatic field generated by the latter. Thus, with the helix bundle alone, the electrostatic energy minimum is ca. −1.9 kcal mol^{-1} and the profile below $-RT$(−0.6 kcal mol^{-1}) ranges from z ca. −18 Å to +19 Å, i.e. about the limits of the bundle per se. In contrast, the presence of the uncharged cylinder deepens the energy minimum to ca. −2.8 kcal mol^{-1} and extends the region of the profile deeper than $-RT$ to z ca. −28 Å to +36 Å. Thus, even in the absence of surface charge the electrostatic potential well becomes deeper and longer. If one assumes the maximum surface charge on the cylinder, the well deepens to ca. −3.8 kcal mol^{-1} and is extended right to the extracellular mouth of the vestibule at z ca. +70 Å. Thus, the assumptions one makes about the surface charge density of the remainder of the protein have a profound effect on the shape of the potential profile generated by the $M2_5$ helix bundle. For instance, although one might consider the cases of zero and maximum surface charge as being limiting cases, a judicious non-uniform arrangement of surface charge on the cylinder could deepen and lengthen the potential well even further.

Current-voltage curves

Single-channel current-voltage (I/V) curves were calculated on the basis of the $M2_5$ and $M2_5$ + cyl models (see Fig. 2B). These were compared with the (ohmic) I/V relationship if one assumed a zero potential profile. In all of these calculations the diffusion coefficients of cat-

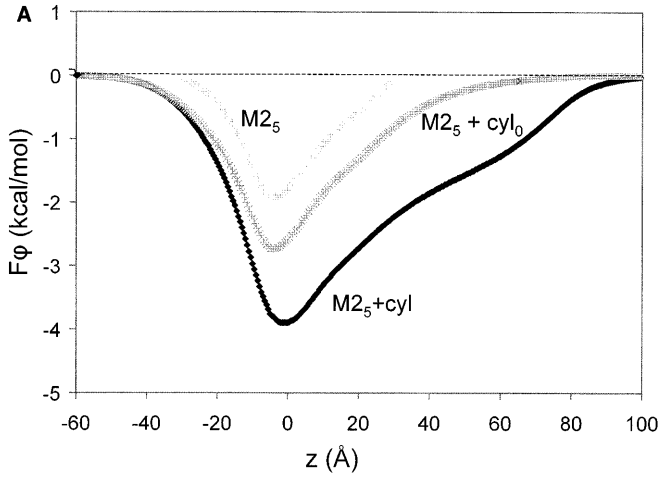

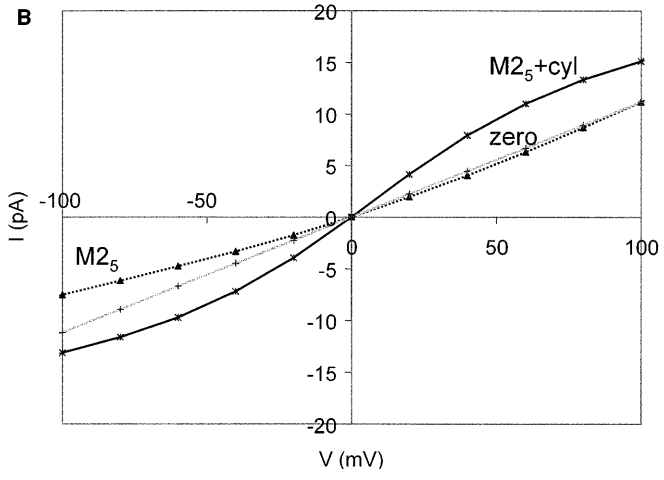

Fig. 2 **A** Electrostatic potential profiles, shown as the electrostatic potential energy of a +1e probe charge ($F\Phi$) as a function of position along the pore (z) axis. The N-terminal (IC) mouth of the pore is at z ca. −20 Å. Profiles are shown for: $M2_5$ = the $M2_5$ helix bundle on its own; $M2_5 + cyl_0$ = the $M2_5$ helix bundle embedded in an uncharged irregular cylinder; and $M2_5 + cyl$ = the $M2_5$ helix bundle embedded in a fully charged irregular cylinder (see text). **B** Calculated single-channel current (I) vs. voltage (V) curves. Curves are shown for: $M2_5$ = the $M2_5$ helix bundle on its own (*dotted line* and ▲); *zero* = a control calculation in which the electrostatic potential due to the protein was assumed to be zero at all points along z (*solid grey line* and +); and $M2_5 + cyl$ = the $M2_5$ helix bundle embedded in a fully charged irregular cylinder (*solid black line* and ×)

ions (D_+) and of anions (D_-) were assumed to be the same ($D = 0.2$ Å^2 ps^{-1}). This is approximately equivalent to the (simulated) diffusion coefficients of K^+ and of Cl^- in bulk aqueous solution (Smith and Sansom 1999). The cross-sectional area of the pore was set to 113 Å^2, this being equivalent to the minimum pore radius of ca. 6 Å. It can be seen that the potential due to the $M2_5$ helix bundle on its own does not appreciably change the calculated I/V curve in the positive voltage quadrant, and only leads to a small reduction in current at negative voltages. The presence of the (charged) cylinder has a more profound effect, increasing the single-channel conductance.

How do these values compare with experimental data? The published value for the single-channel conductance of α7 is ca. 45 pS (Revah et al. 1991). The channel is cation selective. The conductance calculated for the $M2_5$ model is ca. 100 pS and the ion selectivity (measured as I_+/I_-) ranges from 5 to 12 as a function of voltage. For the $M2_5$ + cyl model the calculated conductance is ca. 150 pS, whilst the ion selectivity ranges from 85 to 300. So, it would seem that the $M2_5$ + cyl model is suitably ion selective (given that nAChRs are known to be selective for cations over anions) but the single-channel conductance is about three times higher than the experimental value. However, this value will be very sensitive to, inter alia, the assumed value of D within the pore.

MD simulations

In order to investigate the influence of the cylinder and helix bundle on the behaviour of water within the pore, we ran MD simulations of the $M2_5$ and $M2_5$ + cyl models filled with water molecules. A diagram of the $M2_5$ + cyl + water system is given in Fig. 3. Note that these simulations differ from earlier studies (Smith and Sansom 1997) in that: (1) we have extended the M2 helices to residue −5; (2) we have taken into account the suppression of ionisation of sidechains in the Glu^{+20} ring (Adcock et al. 1998); and (3) we have added the cylinder to the helix bundle model.

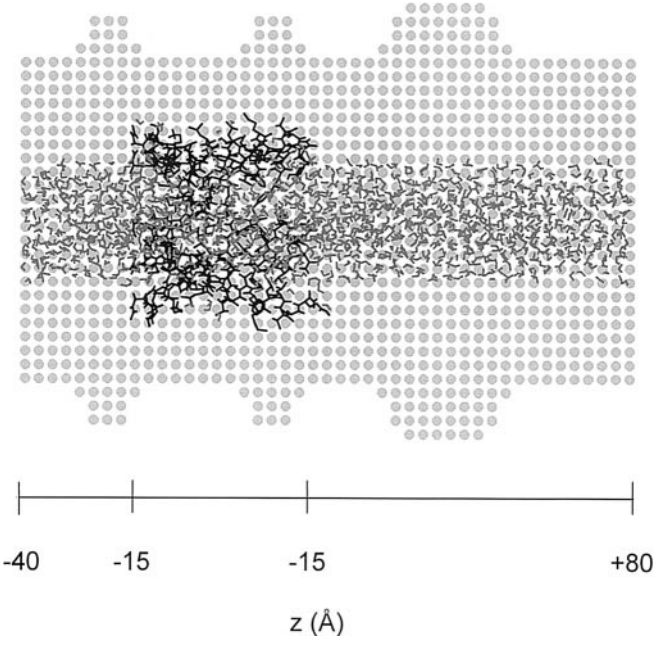

Fig. 3 Diagram of the $M2_5$ + cyl model plus water molecules within the pore. The $M2_5$ bundle is shown in *black* using "bonds" format, the cylinder as *light grey spheres*, and the water molecules as *dark grey bonds*. The approximate z (pore axis) scale is shown below. The intracellular mouth of the cylinder is at z ca. −40 Å

The self-diffusion coefficient of water molecules within the pore is shown in Fig. 4A. Both pore models result in an approximately threefold reduction of the water diffusion coefficient in the narrowest region of the pore relative to the bulk value. The presence of the cylinder results in the reduction of the water diffusion coefficient extending a little way beyond the ends of the helix bundle. It appears that the diffusion coefficient may be somewhat higher than bulk at the extracellular mouth of the cylinder, but we suspect that this is an artefact due to end effects.

Water molecule orientations within the pore can be analysed by plotting the projection of the averaged water molecule dipoles onto the pore axis (Fig. 4B). As in earlier studies (Smith and Sansom 1997), we can see a non-random distribution of water molecule orientations within the pore. In both models ($M2_5$ and $M2_5$ + cyl) the N-terminal dipoles of the helices align the water molecules at the intracellular mouth of the pore. This alignment of water dipoles by helix dipoles is also of interest in the context of the proposed role of helix dipoles on the cavity region of K channels (Roux and MacKinnon 1999). The situation within the remainder of the nAChR pore differs according to the presence versus absence of the cylinder. There appears to be some degree of alignment of the water dipoles within the vestibule of the channel. We anticipate that the exact degree of dipolar alignment will be sensitive to how the cylinder surface charge is treated. However, the extension of the alignment of waters in the $M2_5$ + cyl model into the vestibule is another demonstration of the focusing effect of the cylinder on the electric field due to the M2 segments.

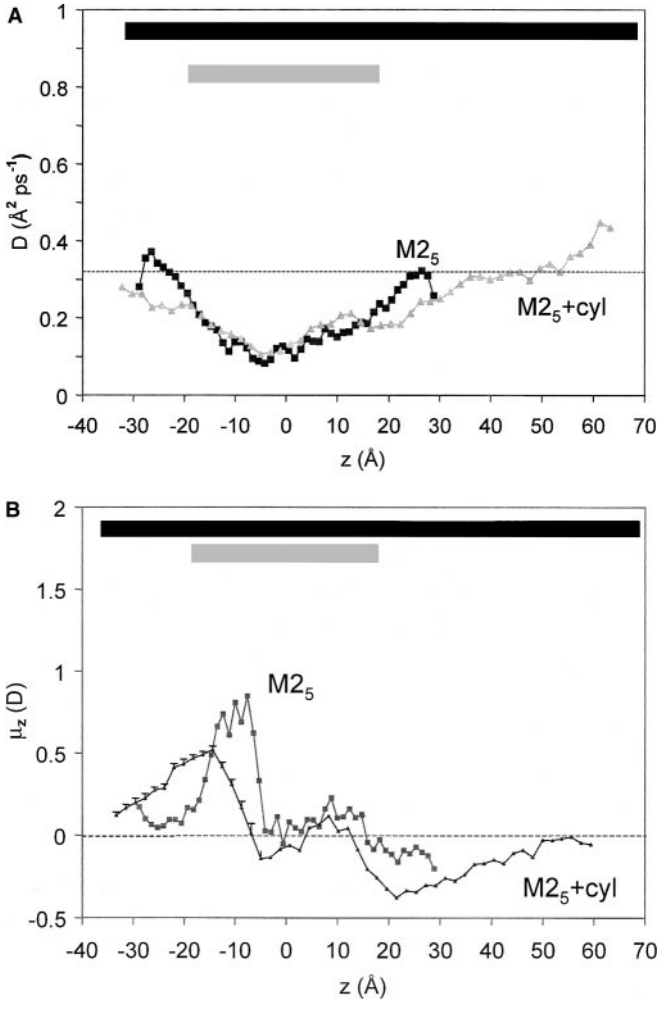

Fig. 4 **A** Water self-diffusion coefficients (D) as a function of z compared for the $M2_5$ (■) and $M2_5$ + cyl (▲) models. Standard errors of the mean (omitted for clarity) range from ca. 0.01 to 0.04 $Å^2$ ps^{-1}) for each point. The approximate extents of the helix bundle and of the cylinder are shown by the *light grey* and *dark grey horizontal bars*, respectively. The *broken horizontal line* shows the value of D for bulk water. **B** Water dipole alignments coefficients as a function of z compared for the $M2_5$ (■) and $M2_5$ + cyl (▲) models. In each case, the average value of the z-projection of the water dipole is shown for each position along the pore axis. The approximate extents of the helix bundle and of the cylinder are shown by the *light grey* and *dark grey horizontal bars*, respectively. Standard errors of the mean (omitted for clarity) range from < 0.05 to ca. 0.15 D for each point

Refining the conductance calculation

The reduction of water diffusion coefficients may be used to obtain an improved estimate of the single-channel conductance. As discussed previously (e.g. Smart et al. 1998), one may obtain a better estimate of a single-channel conductance by assuming that

$$D_{\text{ion}}^{\text{pore}}/D_{\text{ion}}^{\text{bulk}} = D_{\text{water}}^{\text{pore}}/D_{\text{water}}^{\text{bulk}} \tag{3}$$

where the subscripts refer to the diffusing species and the superscripts to its location. Taking a value of ca. 0.3 for this ratio (see Fig. 4A and above) at the narrowest region of the pore gives a revised prediction of 0.3×150 pS $= 45$ pS for the conductance of the $M2_5$ + cyl model, i.e. in good agreement with the experimental value. Thus, from this model one may predict both the single-channel conductance and the cation selectivity of the $\alpha 7$ nAChR with reasonable accuracy. Of course, in this calculation we have employed both the pore cross-sectional area and the reduction in water diffusion at the narrowest point in the channel. We have also assumed that ion diffusion rates (Smith and Sansom 1998, 1999) are reduced by the same amount as water diffusion rates, which may not be exactly so. However, the agreement is encouraging and suggests that the overall approach is suitable for first approximation prediction of single-channel properties from a channel model, at least for those channels for which it is realistic to approximate ion permeation as a diffusion-like process. One might suspect that this overall approach would be less accurate, for example, for a K^+ channel in which the interactions between the pore and the permeant ion are likely to be somewhat stronger as a result of the narrow pore, which has minimum radius of ca. 1 Å in the vicinity of the rings of carbonyl oxygens which form the selectivity filter (Doyle et al. 1998).

MD simulations of pore/water/Na^+

In order to obtain a further perspective of the interaction of ions with the model pore, a series of short (15 ps) MD simulations were carried out in which a Na^+ ion was placed at successive positions along the pore axis. From such simulations one may extract the potential energy of interaction of the Na^+ ion with the remainder of the system and with the components ($M2_5$ bundle, cylinder and water) of the remainder of the system (Fig. 5). From these profiles, one can see that, as in a number of other such calculations for ion channel models (Grice et al. 1997; Smith and Sansom 1997), the Na^+/water and Na^+/pore interaction energy profiles mirror one another, such that the favourable interaction of the ion with the pore is counterbalanced by a less favourable interaction between ion and water in that region. The contribution of the cylinder to the interaction is rather small other than in the vestibule. Overall, the Na^+/all profile is relatively flat and is everywhere negative, favouring a cation within the pore.

One should note the difference in scale between the MD potential energy profiles and the continuum potential energy profiles. In part this reflects the inclusion of counterion screening, owing to inclusion of 100 mM electrolyte within the pore in the continuum electrostatics calculations. However, if one omits such screening, then the calculated I/V curve gives a single-channel conductance of ca. 1000 pS. Evidently, the exact extent of counterion screening (which owing to the inclusion of a Stern radius is mainly operative within the wider, i.e. vestibular, regions of the channel) has a significant effect on the calculated single-channel conductance. Thus, this comparison highlights some of the limitations of both the continuum calculations and the current MD simulations that include only a single Na^+ ion within the pore. In particular, the total depth of the potential energy well at the intracellular mouth of the helix bundle in Fig. 5 is ca. 50 kcal mol^{-1}. This is rather deep. In reality, the presence of counterions and calculation of the free energy profile may modify this picture somewhat in the future. We suspect that the true situation is somewhere between the two extremes represented by the MD and continuum calculations. One possible approach to this problem lies in the work of Eisenberg and colleagues (Chen and Eisenberg 1993a, b; Chen et al. 1997). Another is to run extended (multi-nanosecond) MD simulations in which all components of the system (pore, water, cations, anions, bilayer, transbilayer voltage) are included and in which long-range electrostatic interactions are fully taken into account, e.g. by Ewald summation. This might provide a more accurate picture of the strength of interaction of permeant ions with the channel and with one another.

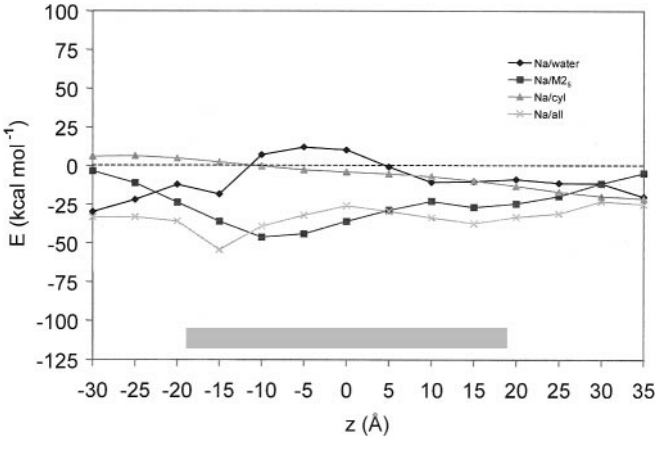

Fig. 5 Na^+ ion interaction potential energy as a function of position along the $M2_5$ + cyl pore. The Na^+/water (◆), $Na^+/M2_5$ (■), Na^+/cylinder (▲) and Na^+/(water + $M2_5$ + cyl) (×) interaction energies are each shown. The *grey bar* indicates the extent of the helix bundle

Conclusions

The principal limitation of the current approach is the approximate nature of the structural model. However, as the resolution of cryoelectron microscopic studies of the nAChR improves (Miyazawa et al. 1999) this will become less problematic. In particular, the emergence of higher resolution images of the transbilayer pore region may improve estimates of the cross-sectional area profile of the channel. Given recent progress in structure determination of ion channels (Chang et al. 1998; Doyle et al. 1998) and their associated extra-membranous domains and subunits (Cabral et al. 1998; Kreusch et al. 1998; Gulbis et al. 1999), one may be optimistic that further structures will appear in the near future, allowing theoretical approaches for relating ion channel structure to physiological function to be tested on a number of systems.

As well as limitations in the structural model, we are aware that the theory used to predict I/V curves in the current study is relatively crude. In particular, we need to explore the effects of ion self-interaction and polarisation charge terms on our calculations. There are more sophisticated theoretical treatments of ion channel electrostatics (Chen and Eisenberg 1993a, b; Syganow and von Kitzing 1995, 1999a, b; von Kitzing and Soumpasis 1996; Chen et al. 1997) which it will be important to explore in the context of models of the nAChR and related channels. Furthermore, even within the simple framework adopted within the current paper, some treatment of asymmetric electrolytes across a membrane, for example, would be desirable.

Despite these limitations, combining structural modelling with continuum calculations that are parameterised via atomistic simulations seems to provide a promising overall approach to understanding single-channel electrophysiological properties. In particular, our results suggest the possible importance of non-M2 regions in governing the single-channel properties of

nAChR. In this context, we note with interest that recent images of the nAChR at ca. 5 Å resolution (Miyazawa et al. 1999) have suggested an important role for the intracellular, non-M2 regions of the protein in the selectivity mechanism of the channel. This is broad agreement with the results of the current study, which support a role for non-M2 domains in determining open channel electrophysiological properties.

Acknowledgements Our thanks to Nigel Unwin and Pierre Jean Corringer for valuable discussions concerning this work. This investigation was supported by grants from The Wellcome Trust. Our thanks to the Oxford Centre for Molecular Sciences for computer support and facilities.

References

Adcock C, Smith GR, Sansom MSP (1998) Electrostatics and the selectivity of ligand-gated ion channels. Biophys J 75: 1211–1222

Barnard EA (1992) Receptor classes and the transmitter-gated ion channels. Trends Pharmacol Sci 17: 368–374

Bertrand D, Galzi JL, Devillers-Thiéry A, Bertrand S, Changeux JP (1993) Stratification of the channel domain in neurotransmitter receptors. Curr Opin Cell Biol 5: 688–693

Breed J, Sankararamakrishnan R, Kerr ID, Sansom MSP (1996) Molecular dynamics simulations of water within models of transbilayer pores. Biophys J 70: 1643–1661

Brooks BR, Bruccoleri RE, Olafson BD, States DJ, Swaminathan S, Karplus M (1983) CHARMM: A program for macromolecular energy, minimisation, and dynamics calculations. J Comp Chem 4: 187–217

Brünger AT (1992) X-PLOR version 3.1. A system for X-ray crystallography and NMR. Yale University Press, New Haven

Cabral JHM, Lee A, Cohen SL, Chait BT, Li M, MacKinnon R (1998) Crystal structure and functional analysis of the HERG potassium channel N-terminus: a eukaryotic PAS domain. Cell 95: 649–655

Chang G, Spencer RH, Lee AT, Barclay MT, Rees DC (1998) Structure of the MscL homolog from *Mycobacterium tuberculosis*: a gated mechanosensitive ion channel. Science 282: 2220–2226

Changeux JP, Galzi JI, Devillers-Thiéry A, Bertrand D (1992) The functional architecture of the acetylcholine nicotinic receptor explored by affinity labelling and site-directed mutagenesis. Q Rev Biophys 25: 395–432

Chen D, Eisenberg R (1993a) Charges, currents, and potentials in ionic channel of one conformation. Biophys J 64: 1405–1421

Chen D, Eisenberg R (1993b) Flux, coupling, and selectivity in ionic channels of one conformation. Biophys J 65: 727–746

Chen D, Lear J, Eisenberg B (1997) Permeation through an open channel: Poisson-Nernst-Planck theory of a synthetic ionic channel. Biophys J 72: 97–116

Chiu SW, Jakobsson E, Subramanian S, McCammon JA (1991) Time-correlation analysis of simulated water motion in flexible and rigid gramicidin channels. Biophys J 60: 273–285

Chiu SW, Novotny JA, Jakobsson E (1993) The nature of ion and water barrier crossings in a simulated ion channel. Biophys J 64: 98–109

Chung SH, Hoyles M, Allen T, Kuyucak S (1998) Study of ionic currents across a model membrane channel using Brownian dynamics. Biophys J 75: 793–809

Chung SH, Allen T, Hoyles M, Kuyucak S (1999) Permeation of ions across the potassium channel: Brownian dynamics studies. Biophys J 77: 2517–2533

Cooper K, Jakobsson E, Wolynes P (1985) The theory of ion transport through membrane channels. Prog Biophys Mol Biol 46: 51–96

Corringer PJ, Bertrand S, Glazi JL, Devillers-Thiery A, Changeux JP, Bertrand D (1999) Molecular basis of the charge selectivity of nicotinic acetylcholine receptor and related ligand-gated ion channels. In: Wallace B (eds) Gramicidin and related channel-forming peptides. (Novartis Foundation symposium series, vol 225) Wiley, pp 215–230

Davis ME, Madura JD, Luty BA, McCammon JA (1991) Electrostatics and diffusion of molecules in solution: simulations with the University of Houston Brownian dynamics program. Comput Phys Commun 62: 187–197

Dieckmann GR, Lear JD, Zhong Q, Klein ML, DeGrado WF, Sharp KA (1999) Exploration of the structural features defining the conduction properties of a synthetic ion channel. Biophys J 76: 618–630

Doyle DA, Cabral JM, Pfuetzner RA, Kuo A, Gulbis JM, Cohen SL, Cahit BT, MacKinnon R (1998) The structure of the potassium channel: molecular basis of K^+ conduction and selectivity. Science 280: 69–77

Dutzler R, Rummel G, Albertí S, Hernández-Allés S, Phale PS, Rosenbusch JP, Benedí VJ, Schirmer T (1999) Crystal structure and functional characterization of OmpK36, the osmoporin of *Klebsiella pneumoniae*. Structure 7: 425–434

Galzi JL, Changeux JP (1994) Neurotransmitter-gated ion channels as unconventional allosteric proteins. Curr Opin Struct Biol 4: 554–565

Grice A, Kerr ID, Sansom MSP (1997) Ion channels formed by HIV-1 Vpu: a modelling and simulation study. FEBS Lett 405: 299–304

Gulbis J, Mann S, MacKinnon R (1999) Structure of a voltage-dependent K^+ channel beta subunit. Cell 97: 943–952

Hille B (1992) Ionic channels of excitable membranes, 2nd edn. Sinauer, Sunderland, Mass

Hucho F, Tsetlin VI, Machold J (1996) The emerging three-dimensional structure of a receptor: the nicotinic acetylcholine receptor. Eur J Biochem 239: 539–557

Kerr ID, Sankararamakrishnan R, Smart OS, Sansom MSP (1994) Parallel helix bundles and ion channels: molecular modelling via simulated annealing and restrained molecular dynamics. Biophys J 67: 1501–1515

Kienker PK, DeGrado WF, Lear JD (1994) A helical-dipole model describes the single-channel current rectification of an uncharged peptide ion channel. Proc Natl Acad Sci USA 91: 4859–4863

Kitzing E von, Soumpasis DM (1996) Electrostatics of a simple membrane model using Greens-function formalism. Biophys J 71: 795–810

Kraulis PJ (1991) MOLSCRIPT: a program to produce both detailed and schematic plots of protein structures. J Appl Crystallogr 24: 946–950

Kreusch A, Pfaffinger PJ, Stevens CF, Choe S (1998) Crystal structure of the tetramerization domain of the *Shaker* potassium channel. Nature 392: 945–948

Le Novère N, Corringer PJ, Changeux JP (1999) Improved secondary structure predictions for a nicotinic receptor subunit: incorporation of solvent accessibility and experimental data into a two-dimensional representation. Biophys J 76: 2329–2345

Lear JD, Schneider JP, Kienker PK, DeGrado WF (1997) Electrostatic effects on ion selectivity and rectification in designed ion channel peptides. J Am Chem Soc 119: 3212–3217

Lester H (1992) The permeation pathway of neurotransmitter-gated ion channels. Annu Rev Biophys Biomol Struct 21: 267–292

Merritt EA, Bacon DJ (1997) Raster3D: photorealistic molecular graphics. Methods Enzymol 277: 505–524

Miyazawa A, Fujiyoshi Y, Stowell M, Unwin N (1999) Nicotinic acetylcholine receptor at 4.6 angstrom resolution: transverse tunnels in the channel wall. J Mol Biol 288: 765–786

Ortells MO, Lunt GG (1995) Evolutionary history of the ligand gated ion channel superfamily of receptors. Trends Neurosci 18: 121–127

Ortells MO, Barrantes GE, Wood C, Lunt GG, Barrantes FJ (1996) Molecular modelling of the nicotinic acetylcholine receptor transmembrane region in the open state. Protein Eng 10: 511–517

Revah F, Bertrand D, Galzi JL, Devillers-Thiery A, Mulle C, Hussy N, Bertrand S, Ballivet M, Changeux JP (1991) Mutations in the channel domain alter desensitization of a neuronal nicotinic receptor. Nature 353: 846–849

Roux B (1995) Theory of transport in ion channels: from molecular dynamics simulations to experiments. In: Goodfellow J (ed) Computer modelling in molecular biology. VCH, Weinheim, pp 133–169

Roux B (1998) Molecular dynamics simulations of ion channels: how far have we gone and where are we heading? Biophys J 74: 2744–2745

Roux B, Karplus M (1994) Molecular dynamics simulations of the gramicidin channel. Annu Rev Biophys Biomol Struct 23: 731–761

Roux B, MacKinnon R (1999) The cavity and pore helices in the KcsA K^+ channel: electrostatic stabilization of monovalent cations. Science 285: 100–102

Sankararamakrishnan R, Adcock C, Sansom MSP (1996) The pore domain of the nicotinic acetylcholine receptor: molecular modelling and electrostatics. Biophys J 71: 1659–1671

Sansom MSP, Sankararamakrishnan R, Kerr ID (1995) Modelling membrane proteins using structural restraints. Nat Struct Biol 2: 624–631

Sansom MSP, Adcock C, Smith GR (1998) Modelling and simulation of ion channels: applications to the nicotinic acetylcholine receptor. J Struct Biol 121: 246–262

Simonson T, Perahia D (1995) Microscopic dielectric properties of cytochrome *c* from molecular dynamics simulations in aqueous solution. J Am Chem Soc 117: 7987–8000

Smart OS, Coates GMP, Sansom MSP, Alder GM, Bashford CL (1998) Structure-based prediction of the conductance properties of ion channels. Faraday Discuss 111: 185–199

Smith GR, Sansom MSP (1997) Molecular dynamics study of water and Na^+ ions in models of the pore region of the nicotinic acetylcholine receptor. Biophys J 73: 1364–1381

Smith GR, Sansom MSP (1998) Dynamic properties of Na^+ ions in models of ion channels: a molecular dynamics study. Biophys J 75: 2767–2782

Smith GR, Sansom MSP (1999) Effective diffusion coefficients of K^+ and Cl^- ions in ion channel models. Biophys Chem 79: 129–151

Syganow A, Kitzing E von (1995) Integral weak diffusion and diffusion approximations applied to ion transport through biological ion channels. J Phys Chem 99: 12030–12040

Syganow A, Kitzing E von (1999a) The drift approximation solves the Poisson, Nernst-Planck, and continuum equations in the limit of large external voltages. Eur Biophys J 28: 393–414

Syganow A, von Kitzing E (1999b) (In)validity of the constant field and constant currents assumptions in theories of ion transport. Biophys J 76: 768–781

Tikhonov DB, Zhorov BS (1998) Kinked-helices model of the nicotinic acetylcholine receptor ion channel and its complexes with blockers: simulation by the Monte Carlo minimization method. Biophys J 74: 242–255

Toyoshima C, Unwin N (1988) Ion channel of acetylcholine receptor reconstructed from images of postsynaptic membranes. Nature 336: 247–250

Ullmann GM, Knapp EW (1999) Electrostatic models for computing protonation and redox equilibria in proteins. Eur Biophys J 28: 533–551

Unwin N (1993) Nicotinic acetylcholine receptor at 9 Å resolution. J Mol Biol 229: 1101–1124

Unwin N (1995) Acetylcholine receptor channel imaged in the open state. Nature 373: 37–43

Woolley GA, Biggin PC, Schultz A, Lien L, Jaikaran DCJ, Breed J, Crowhurst K, Sansom MSP (1997) Intrinsic rectification of ion flux in alamethicin channels: studies with an alamethicin dimer. Biophys J 73: 770–778